Original Paper

Developmental Neuroscience

Dev Neurosci
DOI: 10.1159/000375489

Received: August 29, 2014
Accepted after revision: January 26, 2015
Published online: April 18, 2015

Differential Local Connectivity and Neuroinflammation Profiles in the Medial Prefrontal Cortex and Hippocampus in the Valproic Acid Rat Model of Autism

Martín Gabriel Codagnone[a, b] María Fernanda Podestá[a, b]
Nonthué Alejandra Uccelli[a, b] Analía Reinés[a, b]

[a]Instituto de Biología Celular y Neurociencias 'Prof. E. De Robertis' (IBCN, CONICET-UBA), Facultad de Medicina and
[b]Cátedra de Farmacología, Facultad de Farmacia y Bioquímica, Universidad de Buenos Aires, Buenos Aires, Argentina

Key Words
Valproic acid · NCAM · PSA-NCAM · Astrogliosis · Microgliosis · Neuronal connectivity

Abstract
Autism spectrum disorders (ASD) are a group of developmental disabilities characterized by impaired social interaction, communication deficit and repetitive and stereotyped behaviors. Neuroinflammation and synaptic alterations in several brain areas have been suggested to contribute to the physiopathology of ASD. Although the limbic system plays an important role in the functions found impaired in ASD, reports on these areas are scarce and results controversial. In the present study we searched in the medial prefrontal cortex (mPFC) and hippocampus of rats exposed to the valproic acid (VPA) model of ASD for early structural and molecular changes, coincident in time with the behavioral alterations. After confirming delayed growth and maturation in VPA rats, we were able to detect decreased exploratory activity and social interaction at an early time point (postnatal day 35). In mPFC, although typical cortical column organization was preserved in VPA animals, we found that interneuronal space was wider than in controls. Hippocampal CA3 (cornu ammonis 3) pyramidal layer and the granular layer of the dentate gyrus both showed a disorganized spatial arrangement in VPA animals. Neuronal alterations were accompanied with increased tomato lectin and glial fibrillary acidic protein (GFAP) immunostainings both in the mPFC and hippocampus. In the latter region, the increased GFAP immunoreactivity was CA3 specific. At the synaptic level, while mPFC from VPA animals showed increased synaptophysin (SYN) immunostaining, a SYN deficit was found in all hippocampal subfields. Additionally, both the mPFC and the hippocampus of VPA rats showed increased neuronal cell adhesion molecule (NCAM) immunostaining together with decreased levels of its polysialylated form (PSA-NCAM). Interestingly, these changes were more robust in the CA3 hippocampal subfield. Our results indicate that exploratory and social deficits correlate with region-dependent neuronal disorganization and reactive gliosis in the mPFC and hippocampus of VPA rats. While microgliosis is spread in these two limbic areas, astrogliosis, although extended in the mPFC, is circumscribed to the CA3 hippocampal subfield. Our work indicates that neu-

KARGER 125

© 2015 S. Karger AG, Basel
0378–5866/15/0000–0000$39.50/0

E-Mail karger@karger.com
www.karger.com/dne

Analía Reinés
Instituto de Biología Celular y Neurociencias 'Prof. E. De Robertis'
(IBCN, CONICET-UBA)
Paraguay 2155 3er Piso, C1121ABG, Buenos Aires (Argentina)
E-Mail areines@ffyb.uba.ar

Downloaded by:
UCSF Library & CKM
169.230.243.252 - 4/23/2015 9:51:46 PM

roinflammation and synaptic alterations do coexist in VPA rats, making this model suitable for studying novel aspects of neuron-glia interactions. Moreover, it suggests that the mPFC and hippocampus might behave differently in the context of the local hyperconnectivity and synaptic hypotheses of autism.
© 2015 S. Karger AG, Basel

Introduction

Autism spectrum disorders (ASD) are a group of developmental disabilities with an early onset characterized by varying degrees of impairment in social interaction and verbal and nonverbal communication and by repetitive and stereotyped movements or interests (American Psychological Association, 2013). Although the neurobiology of ASD is still not clear, it is known that both genes and the environment play an important role in the etiology of these disorders [1].

The behavioral complexity of ASD, characterized by deficits in learning, memory, emotion, and social functioning, suggest underlying multiple brain area alterations [2, 3]. Not surprisingly, limbic areas have been implicated in the physiopathology of autism. For instance, the frontal cortex of postmortem samples exhibits overweight [4], alterations in cortical minicolumn cytoarchitecture [5, 6] and microglial and astroglial activation [7, 8]. In spite of being a key limbic structure, the hippocampus has been less explored. Decreased dendritic branches and neuronal size in the CA3 (cornu ammonis 3) from ASD postmortem brains have been reported, as well as controversial results on changes in hippocampal volume [9–13].

Regarding the cellular and molecular alterations underlying morphological abnormalities found in ASD, early neuroinflammation [7, 14], excitation/inhibition imbalance [15, 16] and atypical brain connectivity [17–21] have been postulated. Moreover, alterations found in adhesion molecules [22–26] and other synaptic proteins [27] classify autism as a synaptopathy [28]. Not only gene variants but also altered brain protein expression of the neuronal cell adhesion molecule (NCAM) have been strongly associated with the pathology of ASD [26, 29].

Prenatal exposure to valproic acid (VPA) is a well-validated animal model of autism, since it mimics major behavioral and neuroanatomical alterations found in ASD [30–32]. Early reports on the VPA model showed cerebellar and brainstem alterations similar to those seen in ASD patients [30, 33], along with reduced social interaction and increased repetitive behaviors [31]. The VPA model has become an excellent tool for exploring candidate brain areas likely to be implicated in the behavioral phenotype of ASD [34]. Most recently, research has focused on the medial prefrontal cortex (mPFC) of VPA animals, where hyperconnectivity, increased long-term potentiation and changes in dendritic arborization across different developmental periods have been revealed [32, 35–39]. However, characterization of the cytoarchitectural, glial and synaptic profiles in the mPFC is still missing. Although the hippocampus of VPA animals seems to be functionally compromised, as revealed by social and spatial deficits [31, 40, 41], changes in dendritic spine density [39] and cytoarchitecture in adulthood [42] are the only evidence reported on hippocampal morphology in this model. An extensive description of both areas is relevant for understanding the neurobiological basis of the VPA phenotype and learning about possible candidates for interventions in ASD. In the present work we aim to study early cellular and molecular changes that might give support to the synaptic hypothesis proposed for ASD and to look for concomitant glial changes. To this aim, we studied – at an early time point when social and exploratory impairments have already been established – the cytoarchitecture and expression pattern of synaptic and glial markers and of key determinants of synaptic adhesion in the mPFC and hippocampus from juvenile VPA animals.

Methods

Animals and Drugs

Wistar rats (Facultad de Ciencias Exactas y Naturales, UBA) were housed in an air-conditioned room (temperature: 20 ± 2°C) and maintained on a 12-hour light/dark cycle with food and water ad libitum. Experiments were carried out in accordance with the Guide for the Care and Use of Laboratory Animals provided by the NIH, USA. The experimental protocols were approved by the Ethics Committee for the Care and Use of Laboratory Animals of the School of Pharmacy and Biochemistry at the University of Buenos Aires (Approval No. 180613-1). Special care was taken to minimize the number of animals used and their suffering.

All chemical substances were of analytical grade. Sodium valproate, cresyl violet, 4',6-diamidino-2-phenylindoledihydrochloride (DAPI) and lectin from *Lycopersicon esculentum* (tomato) conjugated with FITC were purchased from Sigma-Aldrich Inc. Mouse monoclonal anti-NCAM (clone 5B8) and anti-PSA-NCAM (clone 5A5; both Hybridoma Bank), anti-synaptophysin (SYN; Chemicom Inc.), anti-glial fibrillary acidic protein (GFAP; Dako), and anti-NeuN (Millipore-Chemicon) were used, as well as secondary fluorescent antibodies (Jackson ImmunoResearch Laboratory Inc.).

Downloaded by:
UCSF Library & CKM
169.230.243.252 - 4/23/2015 9:51:46 PM

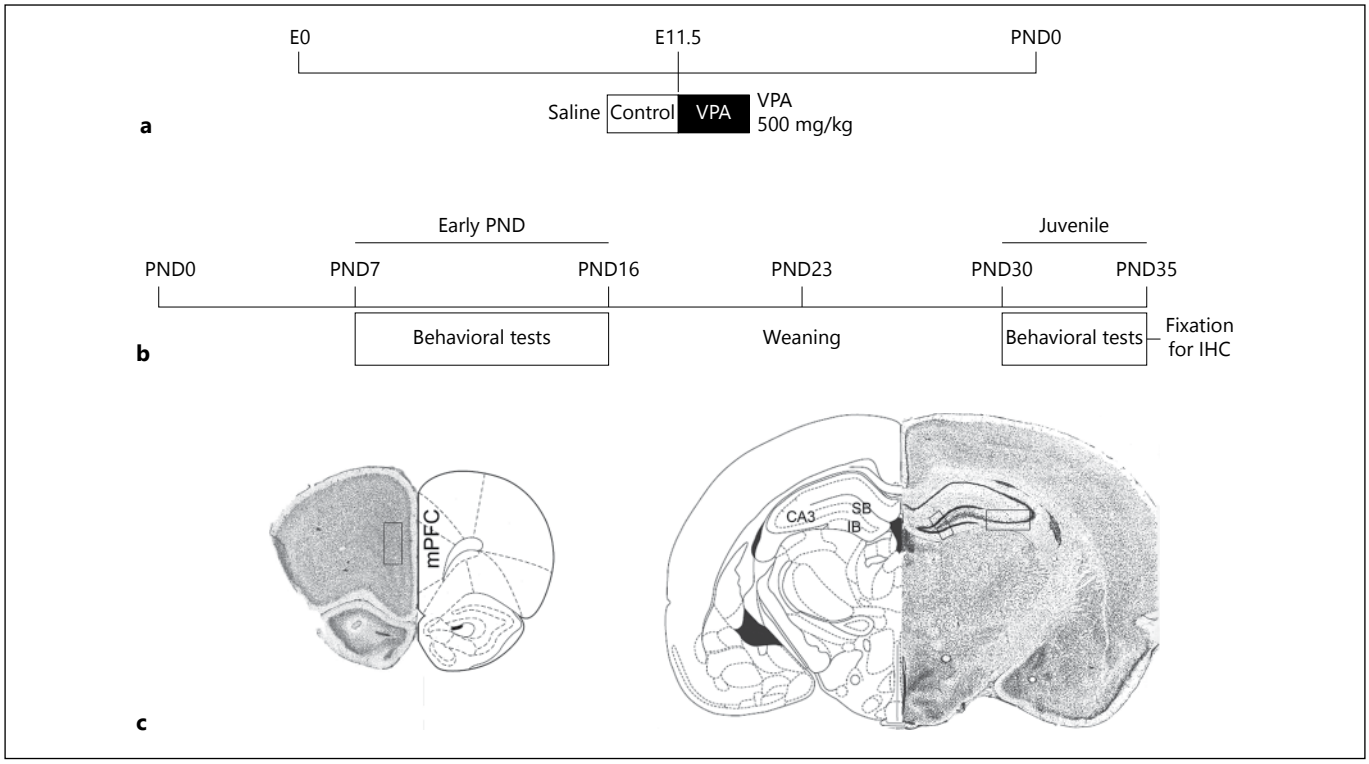

Fig. 1. Schematic representation of the experimental design. IHC = Immunohistochemical. **a** Experimental groups were defined by prenatal pharmacological treatment. Wistar female adult rats were mated overnight and the morning when spermatozoa were found was designated as E0. On E11.5, either 500 mg/kg VPA or saline were administrated intraperitoneally and the corresponding pups assigned to VPA and control groups, respectively. **b** Between PND7 and 16, VPA and control animals were tested for body weight, eye opening, swimming, negative geotaxis, and olfactory discrimination. On PND23, the offspring were separated from the dams and 7 days later (from PND30 to 35) were tested for social interaction and exploratory and repetitive activities. On PND35, VPA and control animals were submitted to fixation procedures for brain immunohistochemical studies. **c** Images of prefrontal and hippocampal slices within the range considered for immunohistochemistry quantification with detailed indications of photographed areas (rectangles). PND = Postnatal day.

VPA Model

VPA Injection during Pregnancy

Nulliparous adult female Wistar rats were mated overnight. The morning when spermatozoa were found was designated as embryonic day 0 (E0). Dams were randomly assigned to either control (n = 4) or sodium valproate (VPA, n = 4) groups. On E11.5 (fig. 1a) females received a single intraperitoneal injection of saline solution (control) or 500 mg/kg VPA according to previous reports [30, 31, 40], with modifications. Sodium valproate was dissolved in saline solution (250 mg/ml) [31]. The females were housed individually and were allowed to raise their own litters until weaning on postnatal day (PND) 23. To confirm the low toxicity of 500 mg/kg VPA, we measured the following parameters. The reabsorption rate (percentage of dams from which a vaginal plug had been detected that did not give birth to a single pup) of the VPA group was 25%, as in Favre et al. [43]. Consequently, the number of VPA dams that gave birth was 3. Dam body mass (DBM) gain during pregnancy [(DBM21 – DBM11)/litter size] was 10.8 + 2.8 g and 10.4 + 2.1 g ($p > 0.05$, Student's t test) for controls and VPA, respectively. Litter size (control 12.2 + 1.7 and VPA 10.5 + 2.8; $p > 0.05$, Student's t test) was not different between treatments, in accordance with Favre et al. [43]. The offspring exhibited good health with no physical malformations. On PND3, the litters were culled to 12 animals, keeping proportion between males and females. Only the males were used for subsequent studies.

Postnatal Growth and Maturation Development

Postnatal growth and maturation development were evaluated according to Schneider and Przewłocki [31]. Evaluation was performed in the light phase (from 11 a.m. to 4 p.m.); 12 control and 8 VPA pups (from 4 and 3 different dams, respectively) were used. Weight gain was measured on PND7, 14 and 23, and eye opening was observed once daily from days 12 to 16 and scored from 0 to 2 according to the number of opened eyes.

Behavioral Analysis

All behavioral experiments were performed in the light phase (11 a.m. and 4 p.m.); 12 control and 8 VPA pups (from 4 and 3 different dams, respectively) were used. Control and VPA animals were treated in the same way and special care was taken to minimize testing time and avoid pup stress.

Downloaded by:
UCSF Library & CKM
169.230.243.252 - 4/23/2015 9:51:46 PM

Early Postnatal Evaluation between PND7 and 16

The pups were subjected to behavioral developmental tests according to St. Omer et al. [44] and Schneider and Przewłocki [31] (fig. 1b). Between PND7 and 10, negative geotaxis was observed once daily. The pups were timed for completing a 180° turn when placed in a head down position on an inclined surface of 25°. A cutoff time of 180 s was set and the pups were given three trials per day. The final score was the average of the three trials.

On PND8, 10, 12, and 16, swimming performance was evaluated in an aquarium filled with water (30 ± 2°C) leveled at 20 cm. Each animal was plunged at the center of the aquarium and observed for 5–10 s. Swimming performance was evaluated according to the position of the nose and head (angle) on the surface of the water. The angle of swimming was rated as follows: 0 = head and nose below the surface; 1 = nose below the surface; 2 = nose and top of head at or above the surface but ears still below the surface; 3 = the same as 2 except that the water line was at mid-ear level, and 4 = the same as 3 except that the water line was at the bottom of the ears. The pups were dried and returned to the home cages [45].

On PND9 and 10, olfactory discrimination was tested. The apparatus consisted of a wooden container of 20 × 8 × 8 cm^3 (length × width × height) with two small plastic bins inside separated by a central platform of 8 × 2 × 0.5 cm^3 (length × width × height) and with a clear plastic cover on top of the container. One bin was filled with clean bedding while the other was filled with averaged 3-day-old home cage bedding. A line was drawn on the plastic cover above the center of each bin. Each pup was placed on the central platform and the latency to enter the home bedding side by crossing the designed line with the front paws and head was timed. Central placement of the pup was balanced by altering the pup facing to or away from the experimenter [46] (fig. 1b).

Behavioral Evaluation at PND30–35

Exploratory activity was assessed in a small open field. The apparatus consisted of a wooden rectangular box of 66 × 57 × 40 cm^3 (length × width × height), with two holes in the shorter and three in the longer walls of the box, located regularly 2 cm over the floor. The number of rearings and hole pokings (when an animal puts its nose inside the hole) was measured during a 3-min session [31].

Social play behavior was assessed in an acrylic plastic circular cage of 36 × 30 cm^2 (diameter × height) with approximately 2 cm of wood shavings covering the floor. The test area was illuminated by a 42-watt red light bulb mounted 50 cm above the floor. On the day of the experiment, the animals were socially isolated for 3.5 h prior to the experiment in order to increase social play [47]. According to the characterization of social deficits in the VPA rat model done by Schneider and Prezwłoki [31] in unfamiliar conditions, the test consisted in placing 2 animals from the same group but different litters and cages into the test cage (VPA vs. VPA; control vs. control). In these unfamiliar conditions, the animals were not habituated but tested for 15 min [31, 48, 49]. Pairs were tested in a randomized order for groups and the animals did not differ by more than 15 g in body weight. Image acquisition was done with a SONY CCD-TRV75 camera recorder placed 60 cm above the test area and connected to a personal computer with AVerTV A833 video capture, while behavior was assessed offline. Latency and number of pinnings (when 1 of the animals is lying with its dorsal surface on the floor of the test cage with the other animal standing over him [31]) and sniffing and social behavior unrelated to social play behavior (following/approaching the test partner and mounting/crawling over the test partner) were measured for each pair of control or VPA animals. For this test, sample size corresponds to the number of analyzed videos, as behavior was quantified by pair of animals and not individually.

To assess repetitive behavior, each animal was placed individually into a dimly illuminated novel open field of 45 × 45 × 20 cm^3 (length × width × height). After a 20-min habituation period, a 10-min video recording started. Offline quantification of self-grooming episodes was performed (fig. 1b).

Histology and Immunostaining

At PND35 the animals were deeply anesthetized (100 mg/kg ketamine hydrochloride and 6 mg/kg xylazine, i.p.), transcardially perfused with heparinized saline solution and fixed with 4% paraformaldehyde in 0.1 M phosphate buffer. Brains were postfixed in the same fixative solution and equilibrated in 0.1 M phosphate buffer containing 25% (w/v) sucrose. The mPFC and hippocampus were serially sectioned in a freezing microtome and the free-floating coronal 30-μm-thick tissue sections were stored at –20°C in 25% (w/v) sucrose in phosphate buffer. These sections were either used to perform cresyl violet staining or blocked with 3% (v/v) normal goat serum for immunostaining [50]. NCAM, GFAP and neuronal-specific nuclear protein (NeuN; 1:2,000), NCAM polysialylated form (PSA-NCAM) and SYN (1:1,000) primary antibodies followed by Rhodamine Red™ or FITC-labeled secondary antibodies, DAPI (1 μg/ml) and tomato lectin (1:1,000) conjugated with FITC were used. Secondary antibody controls were performed in the absence of primary antibodies. NCAM-, PSA-NCAM-, SYN-, and GFAP-positive structures were quantified as relative immunoreactive area (immunoreactive area/total area) [50, 51]. The total area corresponded to the granular and molecular layers in the superior and inferior blades (SB and IB) of the dentate gyrus and to pyramidal and stratum lucidum and radiatum in CA3 (fig. 1c). Images were processed with the ImageJ (NIH) software as described below. Images taken with the microscope were captured with a digital camera and transformed to an 8-bit gray scale, and an interactive threshold selection was carried out as previously described [50, 51]. Briefly, a range of gray value (threshold value) was interactively selected to allow the segmentation of the specific signal from the background. Once the threshold was determined, it was kept fixed for the entire experiment. Following threshold selection, identification of the immunolabeled structures was performed using the software, and finally the area fraction covered by immunostained structures was quantified with the particle counting tool of the ImageJ software. NeuN immunoreactive nuclei were counted as NeuN-positive structures employing the ImageJ cell counter plugin. In the hippocampus, the number of nuclei was measured in the pyramidal and granular cell layers. In the mPFC (fig. 1c), the number of nuclei in the full field of view was considered for neuronal number per unit area measurement. For microglia, tomato lectin-positive structures were quantified as relative immunoreactive area in three spots free of microvasculature per image. Spots were located in the molecular layer of SB and IB and in the stratum lucidum and radiatum of CA3. Single image values corresponded to the average of the three analyzed spots. Only tissue sections corresponding to plates 6–9 (from bregma 4.20 to 2.70) for the mPFC and 29–35 (from bregma –2.80 to –4.30) for the hippocampus of the atlas of Paxinos and Watson [52] were included in the quantifications. An Eclipse 50i Nikon epifluorescence microscope equipped with a Nikon DS-5M cooled camera

Downloaded by:
UCSF Library & CKM
169.230.243.252 - 4/23/2015 9:51:46 PM

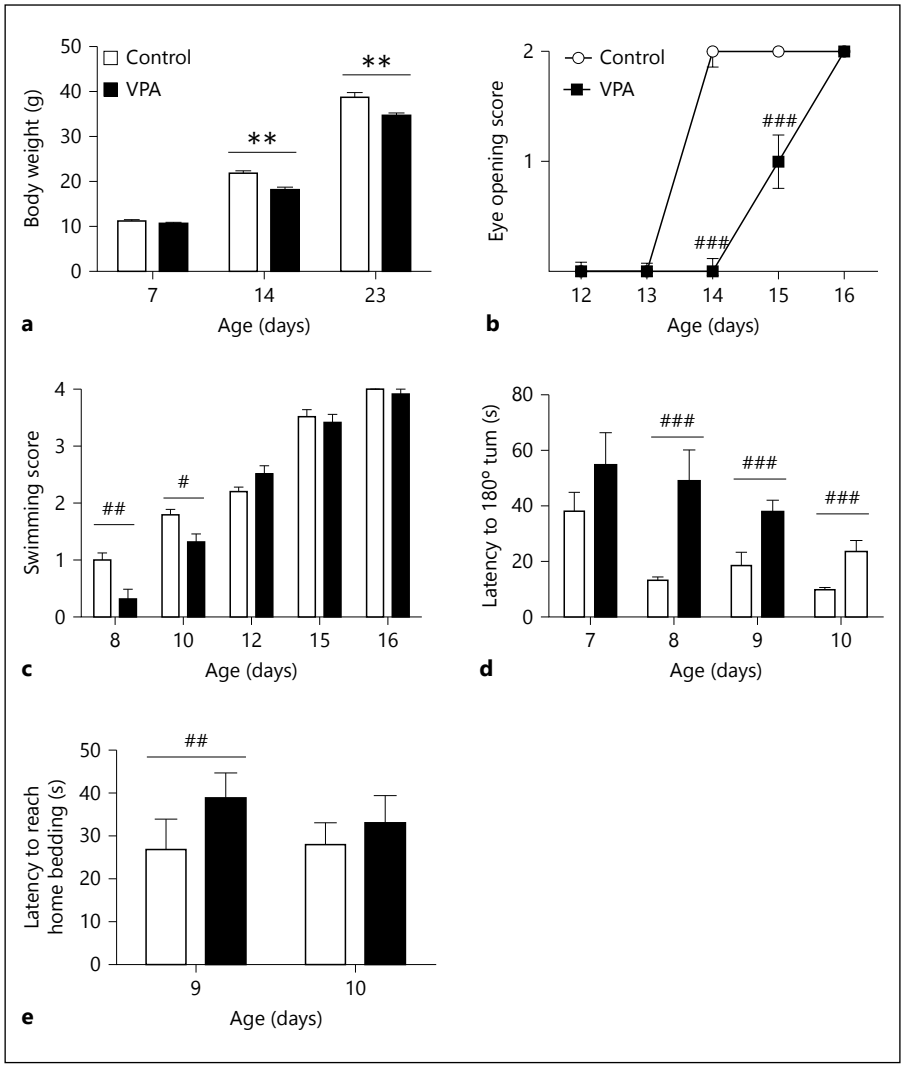

Fig. 2. VPA animals exhibited delayed growth, maturation and behavioral development at early PND. **a** On PND14 and 23, VPA animals showed lower body weight than controls. **b** While control animals had both eyes opened by PND14, it was not until PND16 that VPA rats scored 2 at this test. **c** Swimming was evaluated and VPA animals performed worse than controls on PND8 and 10, while they matched control performance on PND12, 15 and 16. **d** In the negative geotaxis test, VPA rats showed increased latency to a 180° turn from PND8 to 10. **e** VPA animals showed increased latency to reach home bedding on PND9 but not on PND10. Data are expressed as mean values (±SEM; control n = 12, VPA n = 8). $^{\#}$ $p < 0.05$; $^{\#\#}$ $p < 0.05$; $^{\#\#\#}$ $p < 0.001$, between bars by Mann-Whitney U Test. ** $p < 0.01$, between bars by Student's t test.

and a Zeiss Axiophot microscope (Carl Zeiss, Oberkochen, Germany) equipped with an Olympus Q-Color 5 camera were employed. Figures were prepared using Adobe Photoshop 7.0 software (Adobe Systems Inc.). Brightness and contrast were kept constant between the experimental groups.

Results are expressed as mean values (±SEM) of 6 animals per group (from 4 control and 3 VPA different dams). Each immunohistochemistry assay consisted of 6–8 PFC or 5–6 hippocampal serial sections of each animal per group. Each experiment was repeated 2–4 times.

Statistical Analysis

Statistical significance of differences between the control and VPA groups in immunostainings, weight gain, exploratory and repetitive activities, and social behavior was determined by Student's t test. Other behavioral tests (eyes opening, negative geotaxis, swimming test, and olfactory discrimination) were analyzed by the nonparametric Mann-Whitney U test. Statistical significance was set at $p < 0.05$.

Results

Delayed Growth, Maturation and Behavioral Development in VPA Animals

In order to determine early behavioral features of VPA animals, postnatal growth, maturation and behavioral development were evaluated on PND7–16 as schematized in figure 1 in control (n = 12) and VPA (n = 8) animals. VPA rats showed significantly lower body weight on PND14 and 23 ($p < 0.01$), with no difference from controls on PND7 (fig. 2a). A 2-day delay in eye opening was found in the VPA group (fig. 2b). While control pups had both eyes opened by PND14 ($p < 0.001$), it was not until PND16 that VPA animals did so. VPA pups scored lower than control pups at the swimming test on PND8 ($p < 0.01$) and 10 ($p < 0.05$), showing no difference with con-

Downloaded by:
UCSF Library & CKM
169.230.243.252 - 4/23/2015 9:51:46 PM

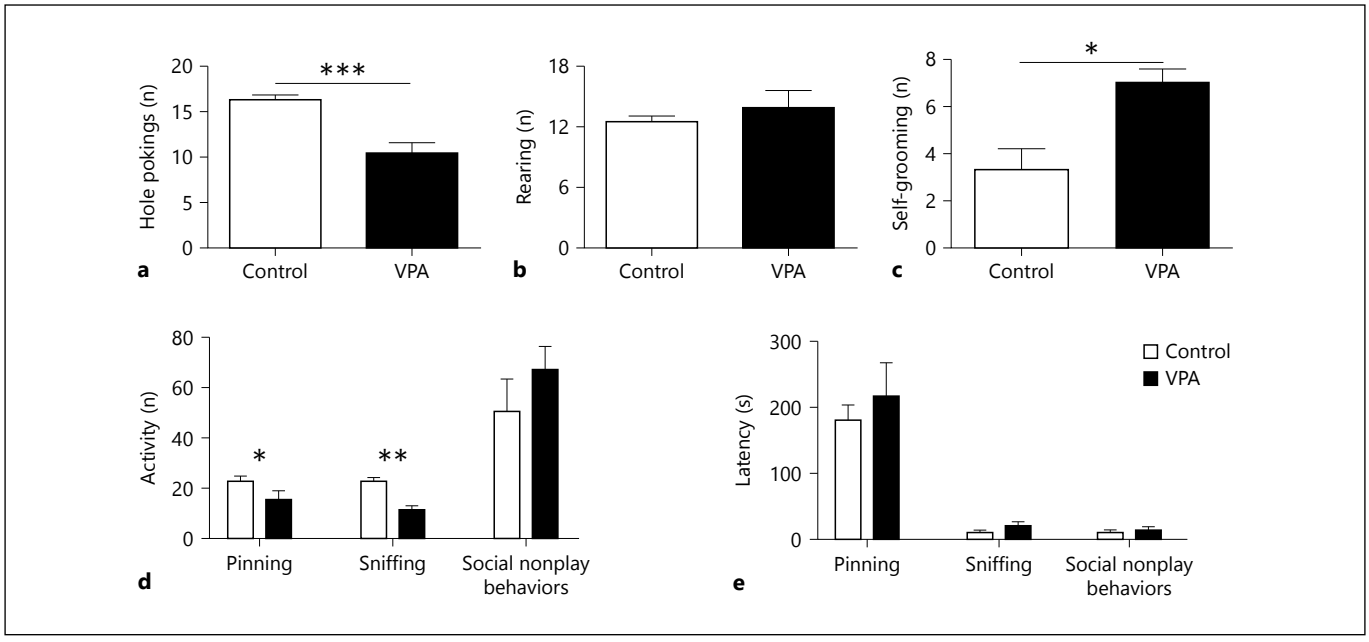

Fig. 3. As early as PND35, VPA animals exhibited reduced exploratory activity and social interaction. VPA animals showed fewer hole pokings (**a**) and a similar number of rearings (**b**) in the exploratory activity test. **c** Increased repetitive self-grooming was found in VPA animals. **d** When paired with the same group but novel partners from a different litter, the VPA group showed reduced frequency of pinnings and sniffing but matching the number of nonplay behaviors. **e** There were no differences in the latency to start pinnings, sniffing or nonplay behaviors. Data are expressed as mean values (±SEM; control n = 12, VPA n = 8 for **a** and **b**; control n = 4, VPA n = 4 for **c**; control n = 9, VPA n = 7 for **d** and **e**). * $p < 0.05$; ** $p < 0.01$; *** $p < 0.001$, between bars by Student's t test.

trol animals afterwards on PND12, 15 and 16 (fig. 2c). When negative geotaxis was evaluated, latency to a 180° turn was higher in VPA animals on PND8, 9 and 10 ($p < 0.001$) but did not differ from controls on PND7 (fig. 2d). VPA animals required more time to reach home bedding on PND9 ($p < 0.01$) but showed no difference on PND10 (fig. 2e). These results indicate delayed maturation, growth and behavioral development in VPA animals.

Exploratory and Social Deficits in VPA Animals Are Revealed as Early as PND35

Exploratory and social impairments are core behavioral deficits of the VPA model [31]. We studied these behavioral alterations at an earlier time point than that previously described by evaluating exploration and social play interaction between PND30 and 35 (fig. 1b). The amount of hole pokings was significantly lower in the VPA animals ($p < 0.01$; control n = 12, VPA n = 8; fig. 3a). The number of rearings did not differ between groups (fig. 3b). Moreover, VPA rats showed increased repetitive self-grooming ($p < 0.05$; control n = 4, VPA n = 4; fig. 3c). Animals from the same group but different litters were paired for the social interaction test. When the number of pinnings was evaluated, the VPA animals exhibited lower social interaction than the controls ($p < 0.05$; control n = 9, VPA n = 7; fig. 3d). There were no differences in the total amount of nonplay behaviors ($p > 0.05$), and sniffing frequency decreased in VPA animals ($p < 0.01$; control n = 9, VPA n = 7; fig. 3d). Similar latencies to pinning, sniffing and nonplay behaviors were found in the VPA and control groups (fig. 3e). Thus, repetitive activity and exploratory and social deficits characteristic of the behavioral phenotype of the VPA model were evident at PND35.

Cytoarchitecture Alterations and Reactive Gliosis in the mPFC of VPA Rats

Although alterations in connectivity and dendritic arborization in the mPFC of VPA animals have been previously reported [35, 39], the histological characteristics of this brain area remain unexplored. To this aim, we evaluated cell organization, neuronal distribution and glial profile in the mPFC of control and VPA animals. Cytoarchitecture of mPFC evaluated by Nissl staining revealed that classical cortical columns were preserved in

Downloaded by:
UCSF Library & CKM
169.230.243.252 - 4/23/2015 9:51:46 PM

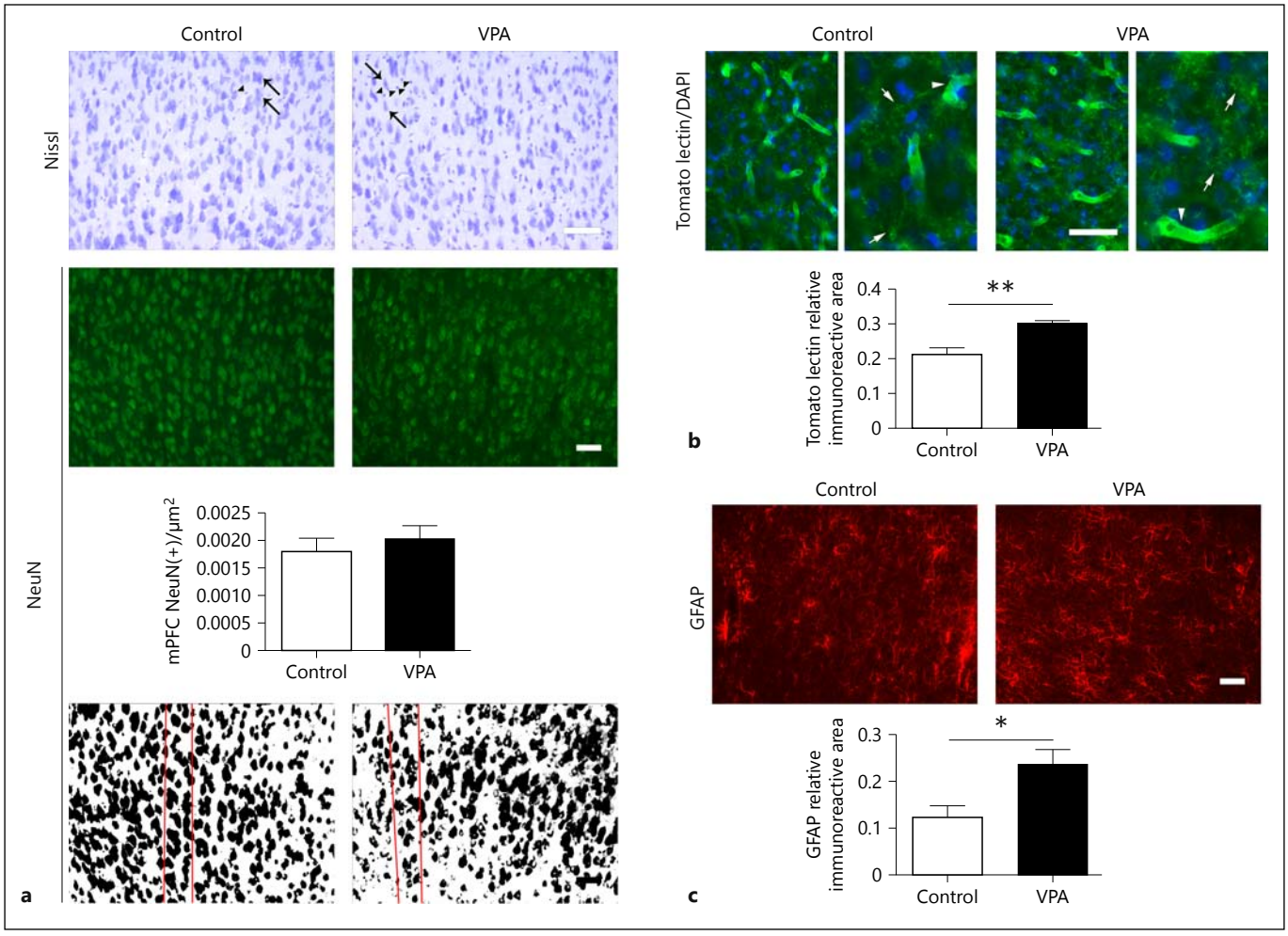

Fig. 4. Characteristic columnar organization and reactive gliosis in the mPFC of VPA animals. **a** Nissl staining and NeuN immunostaining in the mPFC revealed altered columnar cytoarchitecture in VPA animals, particularly showing a broader intercellular space. Quantification of NeuN-positive structures showed no difference in cell number. Arrows point at neuronal nuclei, and arrowheads indicate small nuclei typical of glia lineage. Red lines show cortical columns. **b** Tomato lectin labeling revealed increased microglia in the mPFC of VPA animals. Right panels from each group detail 2× magnification of tomato lectin/DAPI immunostaining. Microgliosis was confirmed by quantification of relative immunoreactive area. Arrows point at microglia labeling, and the arrowhead indicates microvasculature. **c** Increased GFAP immunolabeling was found in the mPFC of the VPA group. Quantification of relative immunoreactive area confirmed the increased GFAP labeling, indicative of reactive astrogliosis. Data are expressed as mean values (±SEM; control n = 6, VPA n = 6). Each experiment was repeated 2–4 times. * $p < 0.05$; ** $p < 0.01$, between bars by Student's t test. Scale bar = 50 μm.

VPA animals. However, neurons were disposed following an atypical spatial arrangement. Particularly, neurons were highly heterogeneous in shape and size, and the intercellular space was wider in VPA animals. NeuN immunostaining confirmed this particular neuronal arrangement in VPA animals (fig. 4a). Determination of neuronal number by NeuN immunostaining showed that the amount of NeuN-positive cells did not significantly differ between groups (fig. 4a), suggesting that a reduction in the number of neurons could hardly contribute to the increased intercellular space seen in VPA animals. In this group, Nissl staining also showed abundant small nuclei corresponding to cells of the glial lineage. Microglia labeling with tomato lectin and astrocyte labeling with GFAP showed increased immunostaining in VPA animals that was confirmed by quantification of relative immunoreactive areas (tomato lectin $p < 0.01$, GFAP $p < 0.05$; control n = 6, VPA n = 6; fig. 4b, c). These findings indicate reactive gliosis in the mPFC of VPA animals.

Downloaded by:
UCSF Library & CKM
169.230.243.252 - 4/23/2015 9:51:46 PM

Altered Cytoarchitecture, Spread Microgliosis and Subregion-Dependent Reactive Astrogliosis in the Hippocampus of VPA Animals

Until now, a few brain areas other than mPFC have been related to the behavioral phenotype of VPA animals. Due to its functional participation in the ontogeny of the altered behaviors, the hippocampus emerges as an area worth exploring. Thus, we studied hippocampal cell organization by Nissl staining, which revealed abnormal cell cytoarchitecture in CA3, IB and SB of VPA animals (fig. 5a). In control animals, the CA3 region showed the classical compact organization with closely packed cells and neat upper and lower limits of the pyramidal layer. VPA animals showed a spread cell arrangement with diffuse boundaries and cell positioning out of the pyramidal layer. Similar alterations were found in the granular layer of the SB and IB of the dentate gyrus. This layer showed less compact cell disposition and diffuse boundaries.

To confirm the neuronal identity of the disorganized cell arrangement, NeuN immunostaining was evaluated (fig. 5b). The number of NeuN-positive cells in the CA3 pyramidal layer of VPA animals was not significantly different from that shown in controls, whereas the CA3 area occupied by these cells was significantly larger ($p < 0.001$; control n = 6, VPA n = 6). Consequently, neuronal number per unit area was lower in the CA3 of VPA animals ($p < 0.01$; control n = 6, VPA n = 6). This parameter was also reduced in the SB and IB of VPA animals (SB $p < 0.05$, IB $p < 0.01$; control n = 6, VPA n = 6). In these hippocampal subregions a trend toward a lower neuronal number in the granular layer was accompanied with no changes in the occupied area.

To assess whether hippocampal glial cells were affected, we studied microglia and astrocytes by tomato lectin and GFAP immunostaining, respectively. VPA animals showed an increased tomato lectin relative immunoreactive area in the three hippocampal subregions (CA3 and SB $p < 0.01$, IB $p < 0.05$; control n = 6, VPA n = 6; fig. 5c). The GFAP relative immunoreactive area increased in CA3 ($p < 0.01$; control n = 6, VPA n = 6) and did not change in the SB or IB of the dentate gyrus of VPA animals (fig. 5d). These results indicate spread hippocampal microgliosis and CA3-specific astrogliosis in the hippocampus of VPA animals.

Contrasting SYN Labeling But Similar High NCAM/PSA-NCAM Expression Ratio between mPFC and Hippocampus of VPA Animals

Taking into account the hypothesis that centers the study of autism on the synapse and our findings concerning the altered neuronal distribution in the VPA model, we studied the expression pattern of the synaptic vesicle protein SYN and of NCAM, an adhesion molecule found altered in autistic patients [26, 29]. In the mPFC, VPA animals showed increased SYN ($p < 0.01$; control n = 6, VPA n = 6; fig. 6a) and NCAM ($p < 0.001$; control n = 6, VPA n = 6; fig. 6b) together with reduced PSA-NCAM relative immunoreactive areas ($p < 0.01$; control n = 6, VPA n = 6; fig. 6c) compared to control animals. Concerning SYN immunostaining and in contrast to what we described in mPFC, the SYN relative immunoreactive area decreased in all the studied hippocampal subregions of VPA animals ($p < 0.001$; control n = 6, VPA n = 6; fig. 7a). NCAM immunostaining increased in the CA3 region ($p < 0.001$; control n = 6, VPA n = 6) and was unchanged in the SB and IB of the dentate gyrus (fig. 7b). On the other hand, PSA-NCAM immunoreactivity decreased in CA3 ($p < 0.001$; control n = 6, VPA n = 6) and the IB ($p < 0.01$; control n = 6, VPA n = 6) of VPA animals but it was similar to controls in the SB (fig. 7c). Conse-

Fig. 5. Altered cytoarchitecture, spread microgliosis and subregion-dependent astrogliosis in the hippocampus from VPA animals. pyr = Pyramidal cell layer; gra = granular layer. **a** Nissl staining in CA3, SB and IB areas revealed abnormal cell cytoarchitecture in the hippocampus of VPA animals. In CA3, the cells distributed laxly in the pyramidal layer, creating nondefined upper and lower boundaries. Similarly, SB and IB granular layers had a less compact organization and diffused limits. **b** NeuN immunostaining in CA3, SB and IB areas of the hippocampus showed the same neuronal organization pattern as that revealed by Nissl staining. Quantification of NeuN-positive structures showed no differences in neuronal number in any hippocampal subregion. In the CA3 of the VPA group, the occupied area increased, thus rendering a decreased number of neurons per CA3 unit area. In the SB and IB of VPA animals, the neuronal-occupied area showed no statistical difference, but neuronal number per granular unit area decreased. **c** Increased microglial cell labeling with tomato lectin in all studied hippocampal subregions of VPA animals. Right panels show 2× magnification of tomato lectin/DAPI immunostaining. Quantification of relative immunoreactive area confirmed hippocampal microgliosis in the VPA group. Arrows point at microglia labeling and the arrowhead indicates microvasculature. **d** Astrocyte immunostaining with GFAP increased in CA3 and remained unchanged in the SB and IB areas of VPA animals. GFAP quantification confirmed CA3-specific astrogliosis in the VPA group. Data are expressed as mean values (±SEM; control n = 6, VPA n = 6). Each experiment was repeated 2–4 times. * $p < 0.05$; ** $p < 0.01$; *** $p < 0.001$, between bars by Student's t test. Scale bar = 50 μm.

(*For figure see next pages.*)

Downloaded by:
UCSF Library & CKM
169.230.243.252 - 4/23/2015 9:51:46 PM

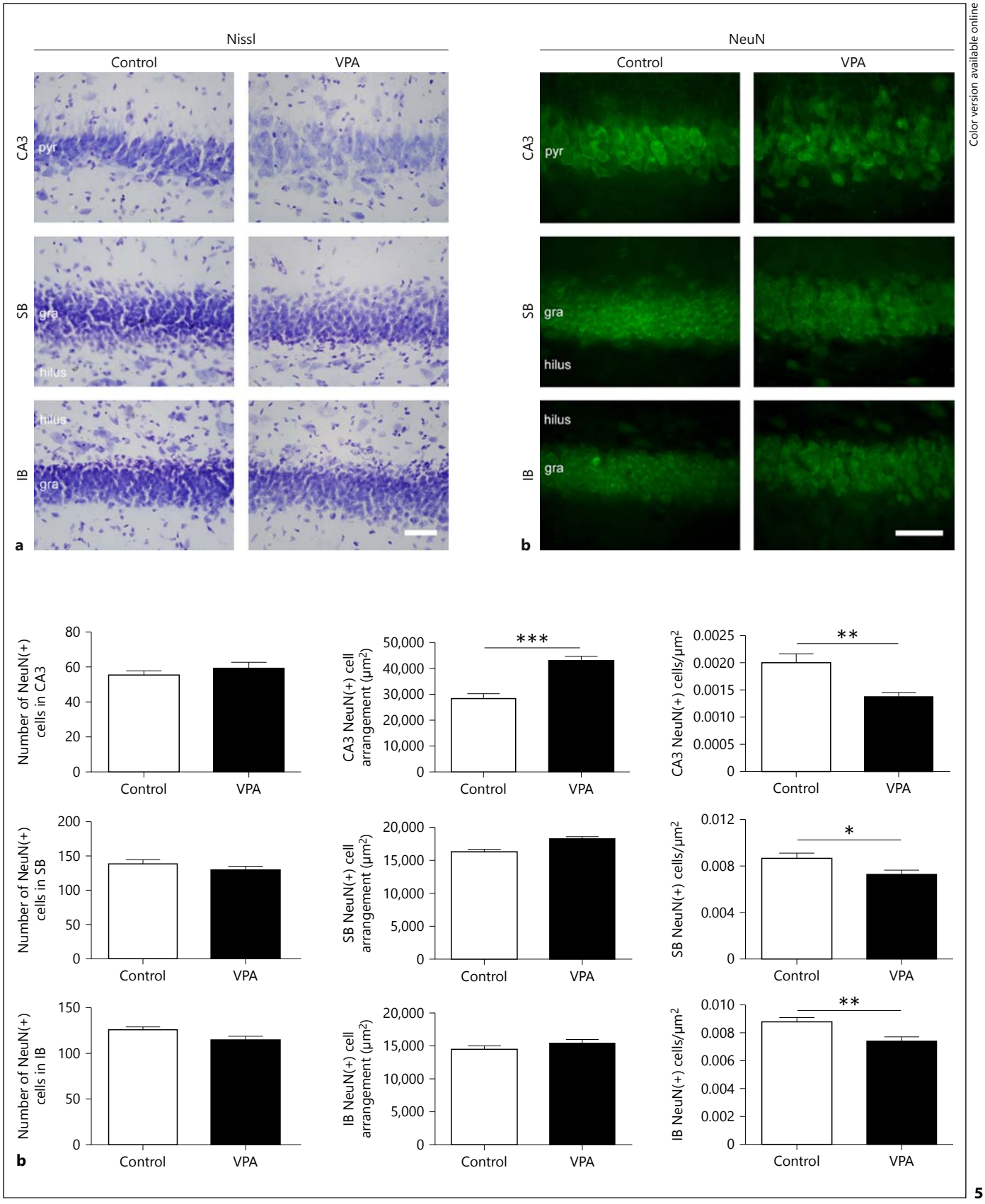

5

Color version available online

Downloaded by:
UCSF Library & CKM
169.230.243.252 - 4/23/2015 9:51:46 PM

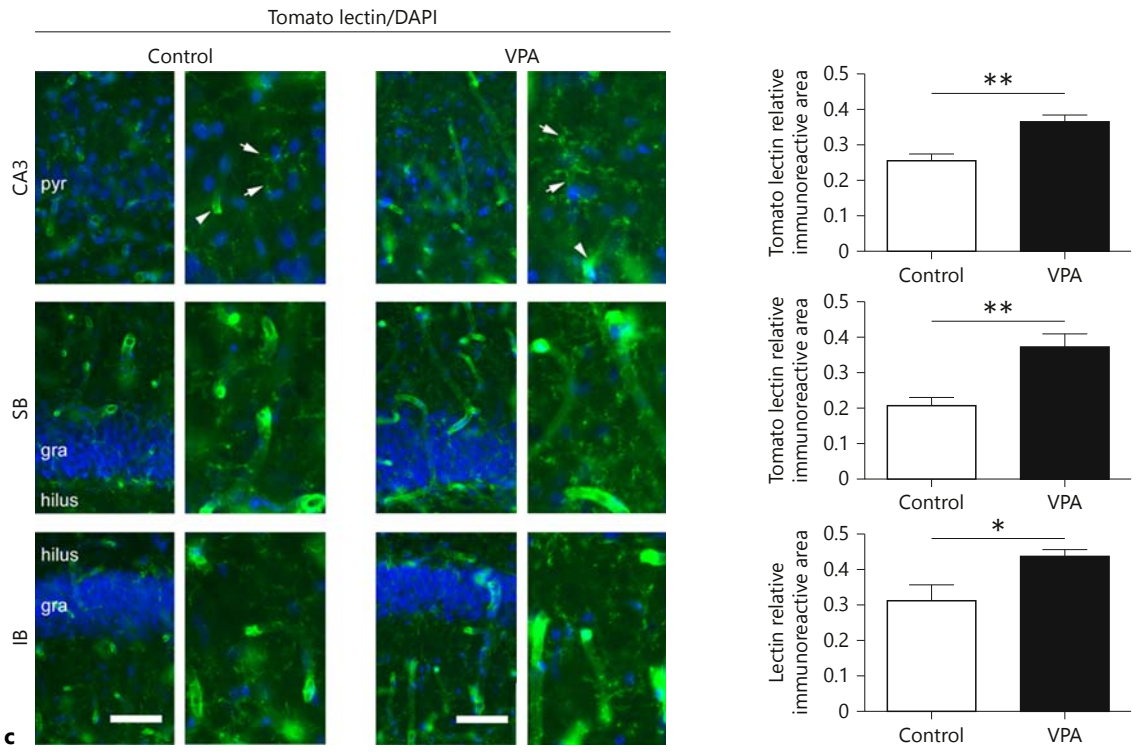

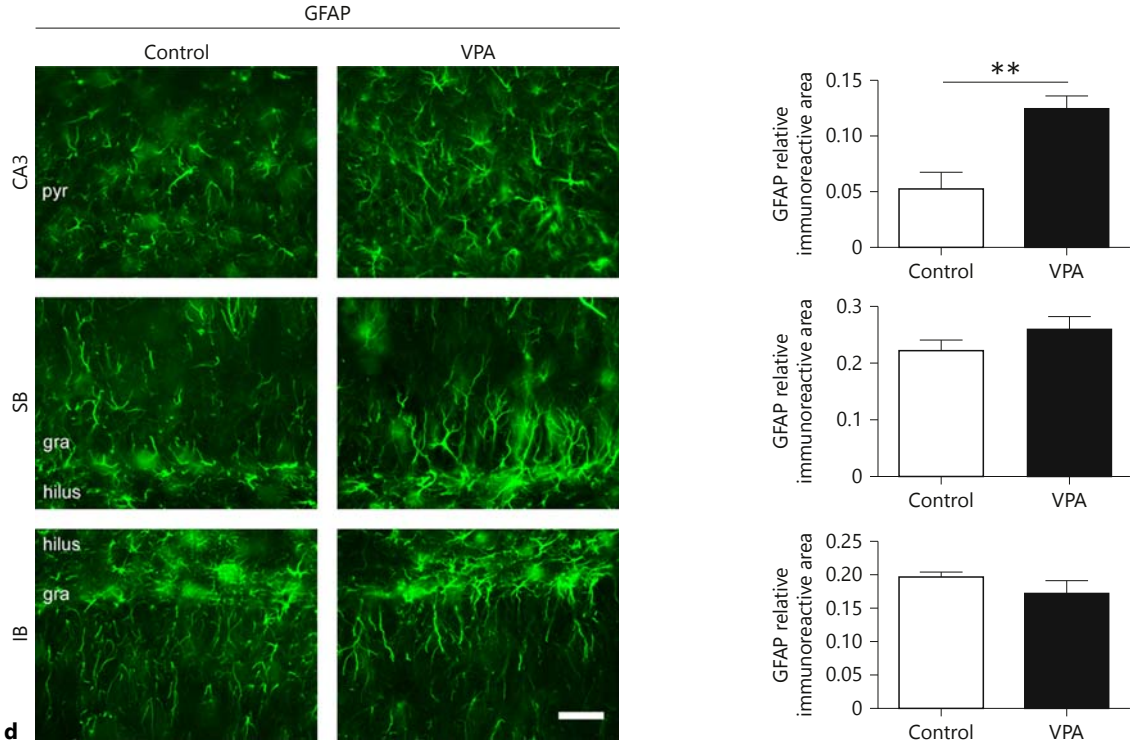

5

Color version available online

Downloaded by:
UCSF Library & CKM
169.230.243.252 - 4/23/2015 9:51:46 PM

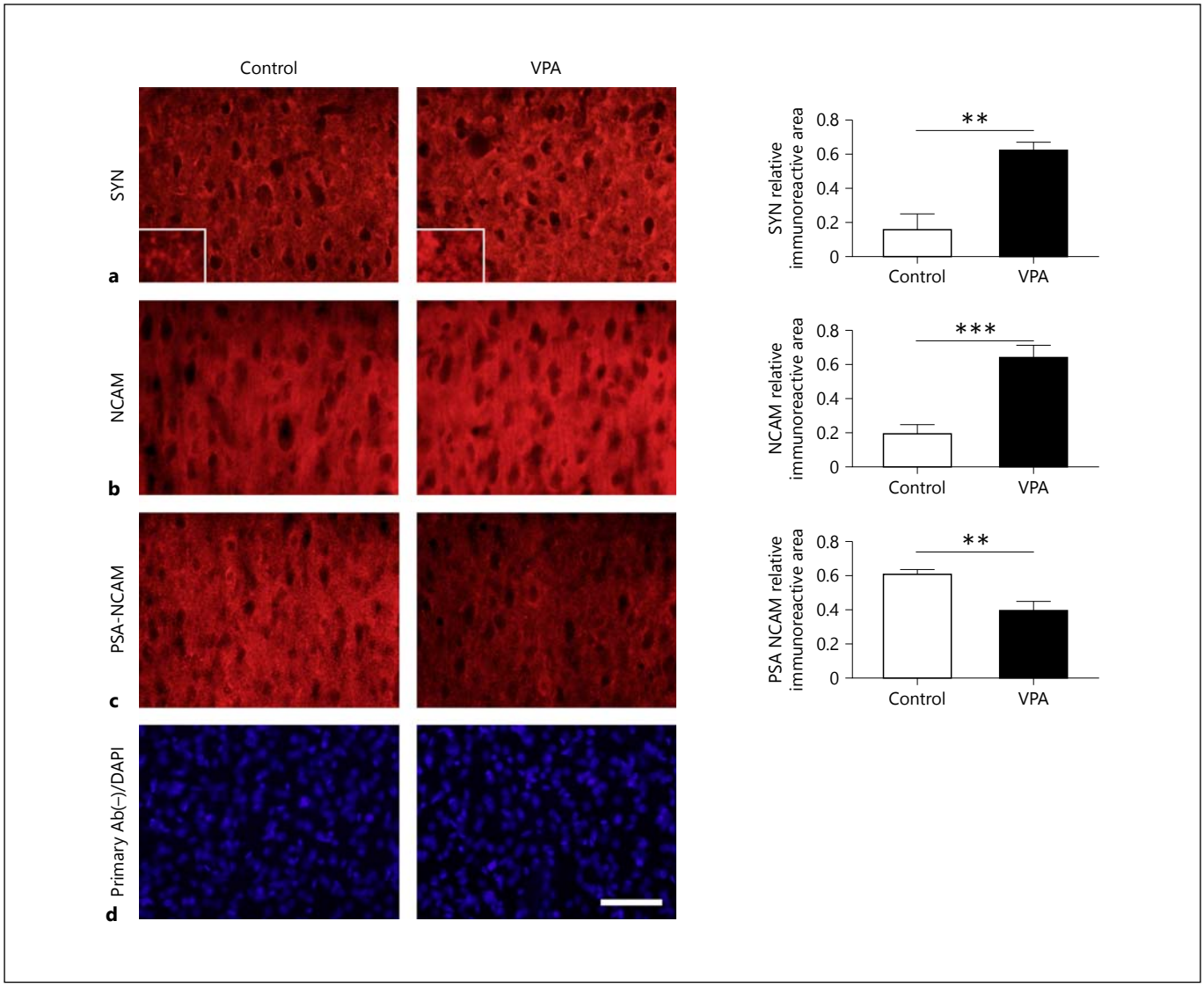

Fig. 6. Increased synaptic marker expression and NCAM/PSA-NCAM ratio in the mPFC of VPA animals. Ab = Antibody. SYN (**a**) and NCAM (**b**) immunostainings increased in the mPFC of VPA animals, as confirmed by quantification of relative immunoreactive area. Insets in **a** correspond to 3× magnification of SYN immunostaining. **c** PSA-NCAM immunostaining clearly decreased in the mPFC of VPA animals. Quantification confirmed PSA-NCAM relative immunoreactive area reduction in VPA animals. **d** Microphotographs of secondary antibody negative controls show DAPI labeling and lack of red immunofluorescence in the absence of NCAM primary antibody. The same results were obtained in the absence of SYN and PSA-NCAM primary antibodies. Data are expressed as mean values (±SEM; control n = 6, VPA n = 6). Each experiment was repeated 2–4 times. ** $p < 0.01$; *** $p < 0.001$, between bars by Student's t test. **a–c** Scale bar = 50 μm. **d** Scale bar = 65 μm.

Fig. 7. Hippocampal SYN deficit is accompanied with subregion-specific NCAM/PSA-NCAM ratios in VPA animals. pyr = Pyramidal cell layer; sl = stratum lucidum; sr = stratum radiatum; gra = granular layer; sgra = subgranular layer. **a** Decreased SYN immunostaining in CA3, SB and IB areas of the hippocampus of VPA animals. SYN reduction was confirmed by relative immunoreactive area quantification. Insets (3× magnification) detail SYN immunostaining pattern. **b** NCAM immunostaining increased in CA3 and remained unaltered in the SB and IB of VPA animals, as confirmed by relative immunoreactive area quantification. **c** PSA-NCAM immunostaining and relative immunoreactive area decreased in CA3 and IB and were unchanged in the SB of VPA animals. Data are expressed as mean values (±SEM; control n = 6, VPA n = 6). Each experiment was repeated 2–4 times. ** $p < 0.01$; *** $p < 0.001$, between bars by Student's t test. Scale bar = 50 μm.

(*For figure see next pages.*)

Downloaded by:
UCSF Library & CKM
169.230.243.252 - 4/23/2015 9:51:46 PM

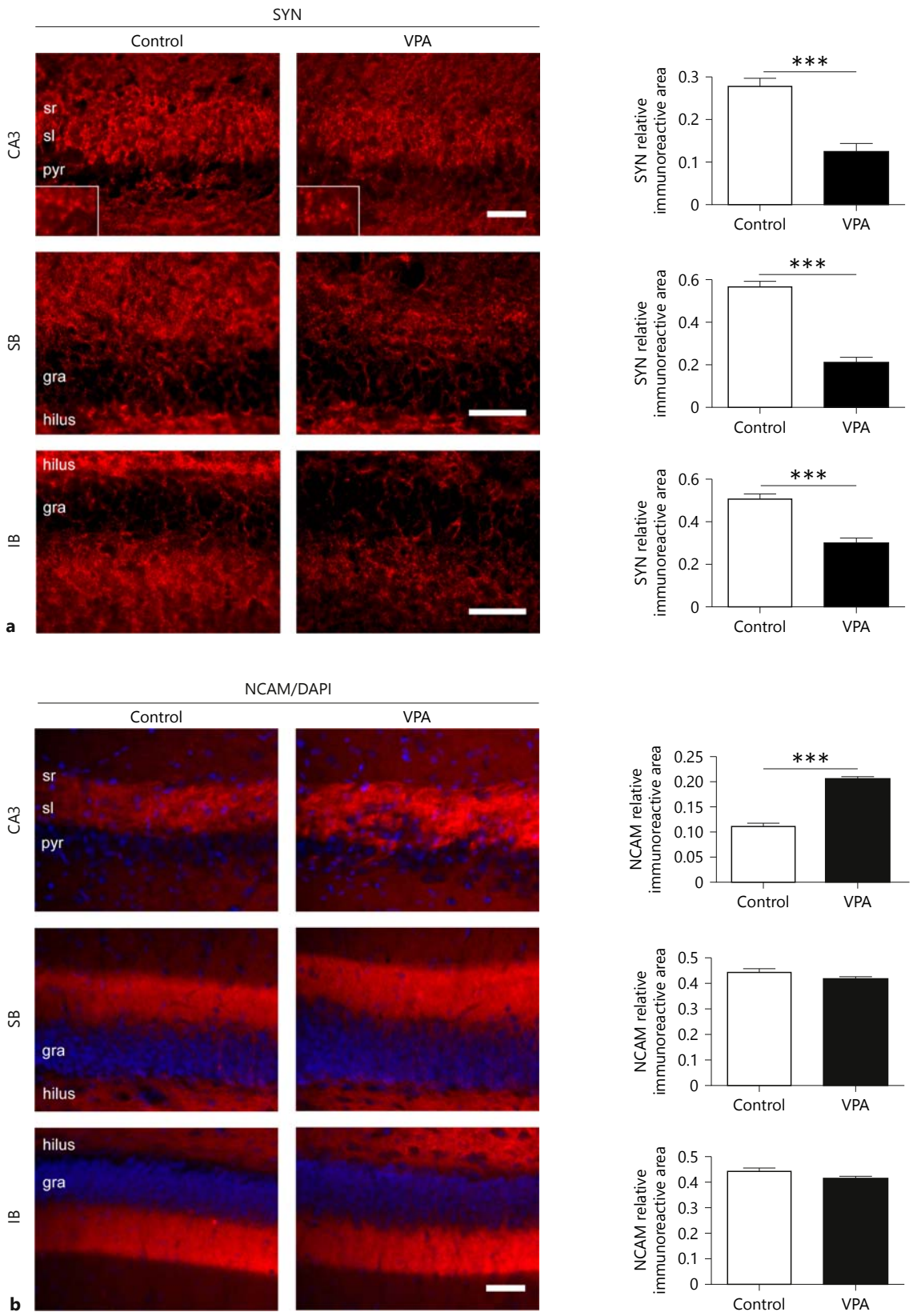

7

Color version available online

Downloaded by:
UCSF Library & CKM
169.230.243.252 - 4/23/2015 9:51:46 PM

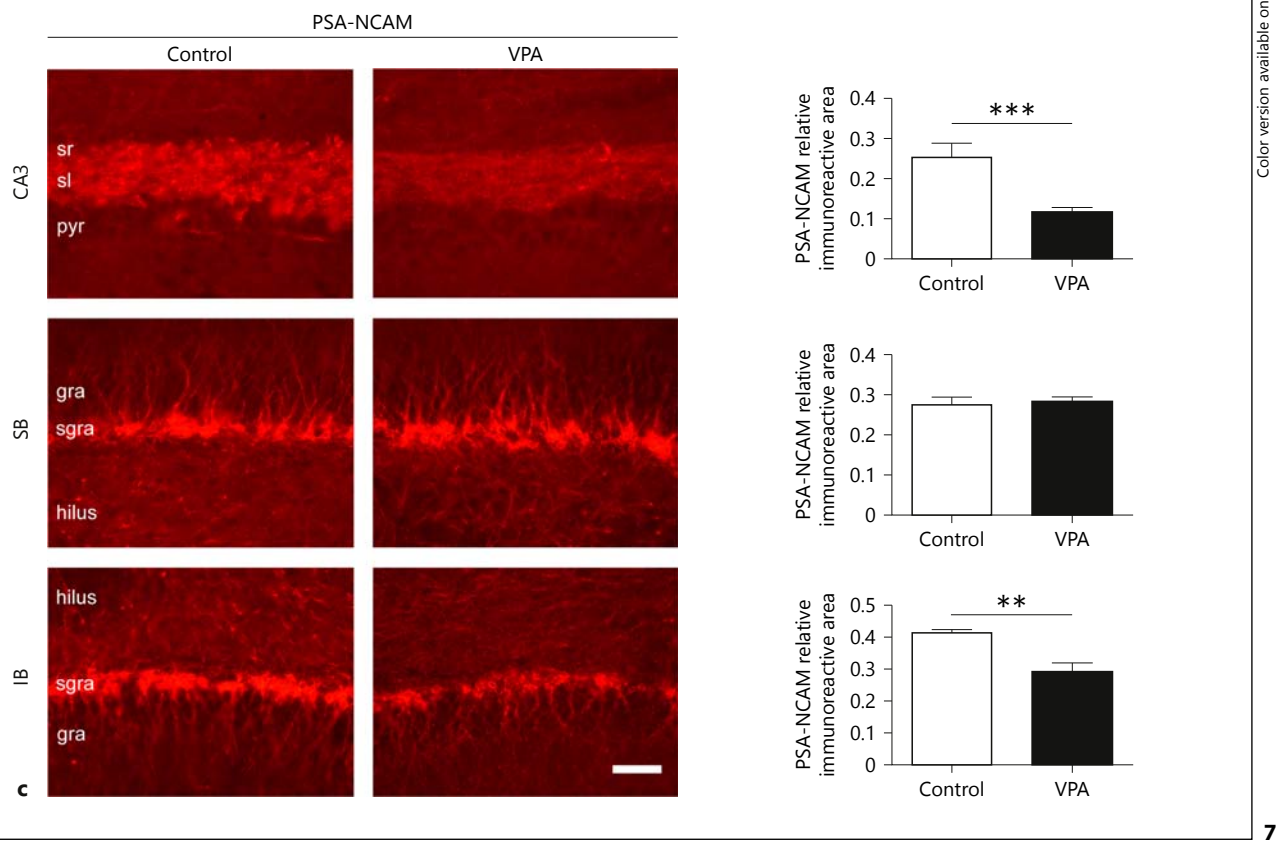

Color version available online

7

quently, the hippocampal NCAM/PSA-NCAM expression ratio increased in CA3 and IB but was unchanged in the SB of VPA animals.

Discussion

In the present work, we explored the complexity of ASD from a histochemical point of view by characterizing brain areas relevant to the behavioral phenotype of the VPA rat model of autism. We searched for early structural and molecular changes in the mPFC and hippocampus that would be coincident in time with the behavioral alterations of the VPA model. With this aim, we firstly confirmed growth, maturation and behavioral development delay in the VPA rats between PND7 and 16 and then performed our study as early as social and exploratory deficits could be documented (PND30–35). There have been previous reports by Schneider and Przewłocki [31], who described these impairments but in a time window ranging from PND30 to 50. In comparison, in the present work we were able to demonstrate social and exploratory deficits at an earlier and narrower postnatal period (PND30–35), a finding that was crucial to define our time point for cellular and morphological evaluation.

Several brain areas have been implicated in the behavioral alterations described in ASD patients. Not surprisingly, due to its well-known integrative function, abnormalities in the PFC have been highly associated with communication and social deficits in autism [19]. Postmortem brain samples of autistic patients revealed histological alterations in this area. For instance, minicolumns are characterized by significantly smaller cells and a less compact intracolumnar arrangement [5]. In the present study we show columnar disorganization in the mPFC of VPA rats for the first time, mimicking that described in autistic patients. Moreover, we confirm neuronal participation in the mPFC cytoarchitectural changes. Even though columnar organization is partially preserved in VPA rats, neurons look smaller and sparser, thus rendering a broader interneuronal space. The fact that we were able to document these findings in the medial region of PFC also provides novel evidence that strongly suggests a link be-

Downloaded by:
UCSF Library & CKM
169.230.243.252 - 4/23/2015 9:51:46 PM

tween these structural alterations and the VPA behavioral phenotype.

Despite a thorough knowledge of the role of the hippocampal formation on emotion, motivation and social functioning [53], this region has been poorly explored in autistic patients, and results are contradictory. For instance, MRI studies of patients diagnosed with autism show either increased, decreased or unchanged hippocampal volume [10–13]. Histological reports in postmortem samples described reduced soma size and number of dendritic branches in hippocampal region CA3 [9]. In the hippocampus of autistic patients, Bauman and Kemper [54] showed smaller neurons with increased cell density, while Bailey et al. [55] reported a trend toward a decrease in neuronal density in CA subfields. In our study, VPA rats show evidence of neuronal disorganization in all of the studied hippocampal subregions. Pyramidal and granular cell packing is less compact, and cell layer boundaries are diffuse. Being that the neuronal number remained unchanged, the increased occupied area seems to account for the reduction in the number of neurons per unit area seen in the hippocampus of VPA rats. Consequently, our findings are in agreement with those described by Bailey et al. [55] in autistic patients and support the notion that neuronal disorganization does exist in the hippocampus of VPA rats. On the other hand, to our knowledge there is only one previous report that studied cell organization in the hippocampal subfields of VPA rats, but an increased cell density was found [42]. The discrepancy with our results could be due to the fact that Nissl staining was used in that study, whereas we used NeuN immunostaining, which specifically labels neuron nuclei.

Concomitant with neuronal disorganization, our report is the first to show both reactive microglia and astrocytes in the mPFC and hippocampus of VPA rats. Our findings are in agreement with the microgliosis and astrogliosis described in the PFC [7, 8] and other brain areas [56] of postmortem ASD patients. Furthermore, after finding altered hippocampal glutamate metabolism, Bristot Silvestrin et al. [57] suggested glial compromise in VPA rats. Herein, we not only demonstrate that reactive astrocytes are present in the hippocampus of VPA animals, but we also show microglial reactivity in this area. Interestingly, we provide evidence in favor of a spread reactive microgliosis but CA3-circumscribed astrogliosis. Consequently, cytoarchitectural changes in VPA animals are accompanied with gliosis both in the mPFC and hippocampus, but they differ from each other in terms of the particular pattern. Accordingly, our findings are in line with the neuroinflammation described in autistic patients [7, 8] and highlight the neuroglial cross-talk as an interaction worth studying. Future studies will shed light on whether neuronal and synaptic alterations promote reactive gliosis in the VPA model.

Regarding the alterations in brain connectivity postulated in ASD, it has been proposed that local hyperconnectivity and long-distance hypoconnectivity are key actors in the physiopathology of these disorders [21, 35]. It is worth mentioning that several of the findings that gave rise to the synaptic hypothesis might as well represent the molecular mechanisms underlying these connectivity changes, which were classified by Wass [21] as structural connectivity. For instance, alterations in adhesion molecules have been described in autistic patients [22–26]. Among other relevant findings, mutations in genes encoding NLGN-3/4 and NCAM, as well as altered NCAM brain expression, have been reported in ASD patients [22, 26, 29]. Moreover, the NCAM polysialyltransferase encoded-gene (ST8SIA2) has been pointed out as a noteworthy association for autism [58]. In the VPA model of autism, neuroligin-3 expression has been shown to be decreased [59]. Herein, we studied NCAM and its polysialylated form (PSA-NCAM) in juvenile VPA rats. NCAM participates in synapse formation, maturation and plasticity [60–64], and PSA-NCAM has a role in synapse formation and remodeling [65–67]. Moreover, PSA-NCAM decrease has been shown to deregulate the NMDA receptor [68] and compromise trophic support [69], leading to dendritic and synaptic alterations [70, 71]. Concomitantly with exploratory and social deficits, we interestingly revealed an increased NCAM/PSA-NCAM ratio in the mPFC and hippocampus of juvenile VPA rats. In fact, in most cases, PSA-NCAM expression decreased along with an increase in NCAM levels. In accordance with our results, it has been described that mice lacking polysialyltransferases during development show social interaction deficits [72]. Furthermore, it is worth noting that Foley et al. [41] failed to find differences in the number of PSA-NCAM-positive cells in the dentate gyrus of adult VPA animals. However, in agreement with our findings and based on the lack of increased NCAM polysialylation after a spatial task in VPA animals, the authors suggested a defective regulation of NCAM polysialylation in the dentate gyrus of adult VPA animals.

Intriguingly, the mPFC and hippocampus differ in terms of the synaptic marker SYN. Since SYN levels are associated with synaptic density and/or synaptic vesicle

Downloaded by:
UCSF Library & CKM
169.230.243.252 - 4/23/2015 9:51:46 PM

density [73], our results in the mPFC are in agreement with the local hyperconnectivity described by Rinaldi et al. [35] in this brain region. On the contrary, it is difficult to speculate about the impact of decreased SYN levels together with an increased NCAM/PSA-NCAM ratio on hippocampal connectivity. As discussed by Bringas et al. [39] based on differential mPFC and hippocampal dendritic arborization, it could be proposed that reduced hippocampal SYN expression renders connectivity changes opposed to those found in mPFC. However, increased NCAM levels might act as a functional balance. It should be mentioned that a recent study in VPA animals showed increased SYN expression both in the cerebral cortex and hippocampus [74]. Discrepancies with our findings could be due to the age of the VPA rats, which is not explicitly cited in the report. Overall, it should be noted that when the hippocampus-mPFC pathway is considered [75], local findings should also be contextualized, taking into account long-distance connections [2].

Even more intriguing is the fact that in the hippocampus of VPA rats, some of our findings were subregion dependent. SYN levels were homogeneously decreased regardless of the hippocampal subregion analyzed, but NCAM increased in the most disorganized subregion (CA3). On the other hand, PSA-NCAM reduction was accompanied with reactive astrogliosis. Surprisingly, SB behaved completely differently from the other two subregions, since the NCAM/PSA-NCAM ratio did not change at all. Therefore, it could be postulated that each hippocampal subregion might be differently affected by the particular NCAM/PSA-NCAM balance in the context of decreased SYN levels. Further studies are required to shed light on local hippocampal connectivity.

To sum up, in the present work we have been able to define an early temporal window in which VPA animals exhibit social and exploratory deficits concomitant with morphological and molecular changes in the mPFC and hippocampus, both brain areas highly implicated in the observed behavioral alterations. Our work contributes to the face validity of the VPA model of autism, since we show that the gliosis and structural connectivity alterations described in autistic patients are reproduced in this model. Moreover, the concurrent gliosis and synaptic alterations found in VPA rats may provide more reliable findings in terms of the cellular and molecular bases underlying this complex disorder. Finally, our work provides strong evidence that highlights the hippocampus as a brain area worth exploring in the physiopathology of these disorders. Based on the SYN and NCAM/PSA-NCAM ratio results, our work suggests that the mPFC and hippocampus might behave differently in the context of the local hyperconnectivity and synaptic hypotheses of autism.

Acknowledgments

This work was supported by grants to A. Reinés from Consejo Nacional de Investigaciones Científicas y Técnicas (CONICET; PIP 2010-0937), Agencia National de Promoción Científica y Técnica (ANCYPCT), PICT 2010-2739, and Universidad de Buenos Aires (UBACYT 2012 and 2013), Argentina. We thank Dr. C. Bonavita for English proofreading.

Disclosure Statement

A. Reinés is an investigator from CONICET. The authors declare no conflicts of interest.

References

1 Chaste P, Leboyer M: Autism risk factors: genes, environment, and gene-environment interactions. Dialogues Clin Neurosci 2012; 14:281–292.
2 Müller R-A: The study of autism as a distributed disorder. Ment Retard Dev Disabil Res Rev 2007;13:85–95.
3 Bruining H, de Sonneville L, Swaab H, de Jonge M, Kas M, van Engeland H, Vorstman J: Dissecting the clinical heterogeneity of autism spectrum disorders through defined genotypes. PLoS One 2010;5:e10887.
4 Courchesne E, Pierce K: Brain overgrowth in autism during a critical time in development: implications for frontal pyramidal neuron and interneuron development and connectivity. Int J Dev Neurosci 2005;23: 153–170.
5 Casanova MF, Buxhoeveden DP, Switala AE, Roy E: Neuronal density and architecture (gray level index) in the brains of autistic patients. J Child Neurol 2002;17:515–521.
6 Buxhoeveden DP, Semendeferi K, Buckwalter J, Schenker N, Switzer R, Courchesne E: Reduced minicolumns in the frontal cortex of patients with autism. Neuropathol Appl Neurobiol 2006;32:483–491.
7 Vargas DL, Nascimbene C, Krishnan C, Zimmerman AW, Pardo CA: Neuroglial activation and neuroinflammation in the brain of patients with autism. Ann Neurol 2005;57: 67–81.
8 Tetreault NA, Hakeem AY, Jiang S, Williams BA, Allman E, Wold BJ, Allman JM: Microglia in the cerebral cortex in autism. J Autism Dev Disord 2012;42:2569–2584.
9 Raymond GV, Bauman ML, Kemper TL: Hippocampus in autism: a Golgi analysis. Acta Neuropathol 1996;91:117–119.
10 Aylward EH, Minshew NJ, Goldstein G, Honeycutt NA, Augustine AM, Yates KO, Barta PE, Pearlson GD: MRI volumes of amygdala and hippocampus in non-mentally retarded autistic adolescents and adults. Neurology 1999;53:2145–2150.

Downloaded by:
UCSF Library & CKM
169.230.243.252 - 4/23/2015 9:51:46 PM

11 Schumann CM, Hamstra J, Goodlin-Jones BL, Lotspeich LJ, Kwon H, Buonocore MH, Lammers CR, Reiss AL, Amaral DG: The amygdala is enlarged in children but not adolescents with autism; the hippocampus is enlarged at all ages. J Neurosci 2004;24:6392–6401.
12 Murphy DGM, Beecham J, Craig M, Ecker C: Autism in adults. New biological findings and their translational implications to the cost of clinical services. Brain Res 2011;1380: 22–33.
13 Barnea-Goraly N, Frazier TW, Piacenza L, Minshew NJ, Keshavan MS, Reiss AL, Hardan AY: A preliminary longitudinal volumetric MRI study of amygdala and hippocampal volumes in autism. Prog Neuropsychopharmacol Biol Psychiatry 2014;48:124–128.
14 Theoharides TC, Asadi S, Patel AB: Focal brain inflammation and autism. J Neuroinflammation 2013;10:46.
15 Rubenstein JLR, Merzenich MM: Model of autism: increased ratio of excitation/inhibition in key neural systems. Genes Brain Behav 2003;2:255–267.
16 Blatt GJ, Fatemi SH: Alterations in GABAergic biomarkers in the autism brain: research findings and clinical implications. Anat Rec 2011; 294:1646–1652.
17 Just MA, Cherkassky VL, Keller TA, Minshew NJ: Cortical activation and synchronization during sentence comprehension in high-functioning autism: evidence of underconnectivity. Brain 2004;127:1811–1821.
18 Belmonte MK, Allen G, Beckel-Mitchener A, Boulanger LM, Carper RA, Webb SJ: Autism and abnormal development of brain connectivity. J Neurosci 2004;24:9228–9231.
19 Courchesne E, Pierce K: Why the frontal cortex in autism might be talking only to itself: local over-connectivity but long-distance disconnection. Curr Opin Neurobiol 2005;15: 225–320.
20 Minshew NJ, Keller TA: The nature of brain dysfunction in autism: functional brain imaging studies. Curr Opin Neurol 2010;23:124–130.
21 Wass S: Distortions and disconnections: disrupted brain connectivity in autism. Brain Cogn 2011;75:18–28.
22 Jamain S, Quach H, Betancur C, Råstam M, Colineaux C, Gillberg IC, Bourgeron T: Mutations of the X-linked genes encoding neuroligins NLGN3 and NLGN4 are associated with autism. Nat Genet 2003;34:27–29.
23 Kim H, Kishikawa S, Higgins AW, Seong I, Donovan DJ, Shen Y, Lally E, Weiss LA, Najm J, Kutsche K, Descartes M, Holt L, Braddock S, Troxell R, Kaplan L, Volkmar F, Klin A, Tsatsanis K, Harris DJ, Noens I, Pauls DL, Daly MJ, MacDonald ME, Morton CC, Quade BJ, Gusella JF: Disruption of neurexin 1 associated with autism spectrum disorder. Am J Hum Genet 2008;82:199–207.
24 Wang K, Zhang H, Ma D, et al: Common genetic variants on 5p14.1 associate with autism spectrum disorders. Nature 2009;459:528–533.
25 Betancur C, Sakurai T, Buxbaum JD: The emerging role of synaptic cell-adhesion pathways in the pathogenesis of autism spectrum disorders. Trends Neurosci 2009;32:402–412.
26 Marui T, Funatogawa I, Koishi S, Yamamoto K, Matsumoto H, Hashimoto O, Namba E, Nishida H, Sugiyama T, Kasai K, Watanabe K: Association of the neuronal cell adhesion molecule (NRCAM) gene variants with autism. Int J Neuropsychopharmacol 2009;12: 439.
27 Durand CM, Betancur C, Boeckers TM, Bockmann J, Chaste P, Fauchereau F, Nygren G, Rastam M, Gillberg IC, Anckarsäter H, Sponheim E, Goubran-Botros H, Delorme R, Chabane N, Mouren-Simeoni MC, de Mas P, Bieth E, Rogé B, Héron D, Burglen L, Gillberg C, Leboyer M, Bourgeron T: Mutations in the gene encoding the synaptic scaffolding protein SHANK3 are associated with autism spectrum disorders. Nat Genet 2007;39:25–27.
28 Zoghbi HY: Postnatal neurodevelopmental disorders: meeting at the synapse? Science 2003;302:826–830.
29 Purcell AE, Rocco MM, Lenhart JA, Hyder K, Zimmerman AW, Pevsner J: Assessment of neural cell adhesion molecule (NCAM) in autistic serum and postmortem brain. J Autism Dev Disord 2001;31:183–194.
30 Rodier PM, Ingram JL, Tisdale B, Nelson S, Romano J: Embryological origin for autism: developmental anomalies of the cranial nerve motor nuclei. J Comp Neurol 1996;370:247–261.
31 Schneider T, Przewłocki R: Behavioral alterations in rats prenatally exposed to valproic acid: animal model of autism. Neuropsychopharmacology 2005;30:80–89.
32 Mychasiuk R, Richards S, Nakahashi A, Kolb B, Gibb R: Effects of rat prenatal exposure to valproic acid on behaviour and neuro-anatomy. Dev Neurosci 2012;34:268–276.
33 Ingram JL, Peckham SM, Tisdale B, Rodier PM: Prenatal exposure of rats to valproic acid reproduces the cerebellar anomalies associated with autism. Neurotoxicol Teratol 2000; 22:319–324.
34 Roullet FI, Lai JKY, Foster JA: In utero exposure to valproic acid and autism – a current review of clinical and animal studies. Neurotoxicol Teratol 2013;36:47–56.
35 Rinaldi T, Silberberg G, Markram H: Hyperconnectivity of local neocortical microcircuitry induced by prenatal exposure to valproic acid. Cereb Cortex 2008;18:763–770.
36 Walcott EC, Higgins EA, Desai NS: Synaptic and intrinsic balancing during postnatal development in rat pups exposed to valproic acid in utero. J Neurosci 2011;31:13097–13109.
37 Sui L, Chen M: Prenatal exposure to valproic acid enhances synaptic plasticity in the medial prefrontal cortex and fear memories. Brain Res Bull 2012;87:556–563.
38 Martin HGS, Manzoni OJ: Late onset deficits in synaptic plasticity in the valproic acid rat model of autism. Front Cell Neurosci 2014;8: 23.
39 Bringas ME, Carvajal-Flores FN, López-Ramírez TA, Atzori M, Flores G: Rearrangement of the dendritic morphology in limbic regions and altered exploratory behavior in a rat model of autism spectrum disorder. Neuroscience 2013;241:170–187.
40 Markram K, Rinaldi T, La Mendola D, Sandi C, Markram H: Abnormal fear conditioning and amygdala processing in an animal model of autism. Neuropsychopharmacology 2008; 33:901–912.
41 Foley AG, Gannon S, Rombach-Mullan N, Prendergast A, Barry C, Cassidy AW, Regan CM: Class I histone deacetylase inhibition ameliorates social cognition and cell adhesion molecule plasticity deficits in a rodent model of autism spectrum disorder. Neuropharmacology 2012;63:750–760.
42 Edalatmanesh MA, Nikfarjam H, Vafaee F, Moghadas M: Increased hippocampal cell density and enhanced spatial memory in the valproic acid rat model of autism. Brain Res 2013;1526:15–25.
43 Favre MR, Barkat TR, Lamendola D, Khazen G, Markram H, Markram K: General developmental health in the VPA rat model of autism. Front Behav Neurosci 2013;7:88.
44 St Omer VE, Ali SF, Holson RR, Duhart HM, Scalzo FM, Slikker W: Behavioral and neurochemical effects of prenatal methylenedioxymethamphetamine (MDMA) exposure in rats. Neurotoxicol Teratol 1991;13: 13–20.
45 Schapiro S, Salas M, Vukovich K: Hormonal effects on ontogeny of swimming ability in the rat: assessment of central nervous system development. Science 1970;168:147–150.
46 Gregory EH, Pfaff DW: Development of olfactory-guided behavior in infant rats. Physiol Behav 1971;6:573–576.
47 Niesink RJ, van Ree JM: Short-term isolation increases social interactions of male rats: a parametric analysis. Physiol Behav 1982;29: 819–825.
48 Schneider T, Turczak J, Przewłocki R: Environmental enrichment reverses behavioral alterations in rats prenatally exposed to valproic acid: issues for a therapeutic approach in autism. Neuropsychopharmacology 2006;31: 36–46.
49 Vanderschuren LJ, Niesink RJ, Spruijt BM, Van Ree JM: Effects of morphine on different aspects of social play in juvenile rats. Psychopharmacology 1995;117:225–231.
50 Reinés A, Cereseto M, Ferrero A, Sifonios L, Podestá MF, Wikinski S: Maintenance treatment with fluoxetine is necessary to sustain normal levels of synaptic markers in an experimental model of depression: correlation with behavioral response. Neuropsychopharmacology 2008;33:1896–1908.
51 Aviles-Reyes RX, Angelo MF, Villarreal A, Rios H, Lazarowski A, Ramos AJ: Intermittent hypoxia during sleep induces reactive gliosis and limited neuronal death in rats: implications for sleep apnea. J Neurochem 2010; 112:854–869.

Downloaded by:
UCSF Library & CKM
169.230.243.252 - 4/23/2015 9:51:46 PM

52 Paxinos G, Watson C: The Rat Brain in Stereotaxis Coordinates, ed 4. San Diego, Academic Press, 1986.
53 DeLong GR: Autism, amnesia, hippocampus, and learning. Neurosci Biobehav Rev 1992;16: 63–70.
54 Bauman M, Kemper TL: Histoanatomic observations of the brain in early infantile autism. Neurology 1985;35:866–874.
55 Bailey A, Luthert P, Dean A, Harding B, Janota I, Montgomery M, Rutter M, Lantos P: A clinicopathological study of autism. Brain 1998;121:889–905.
56 Rodriguez JI, Kern JK: Evidence of microglial activation in autism and its possible role in brain underconnectivity. Neuron Glia Biol 2011;7:205–213.
57 Bristot Silvestrin R, Bambini-Junior V, Galland F, Daniele Bobermim L, Quincozes-Santos A, Torres Abib R, Zanotto C, Batassini C, Brolese G, Gonçalves C-A, Riesgo R, Gottfried C: Animal model of autism induced by prenatal exposure to valproate: altered glutamate metabolism in the hippocampus. Brain Res 2013;1495:52–60.
58 Anney R, Klei L, Pinto D, et al: A genome-wide scan for common alleles affecting risk for autism. Hum Mol Genet 2010;19:4072–4082.
59 Kolozsi E, Mackenzie RN, Roullet FI, DeCatanzaro D, Foster JA: Prenatal exposure to valproic acid leads to reduced expression of synaptic adhesion molecule neuroligin 3 in mice. Neuroscience 2009;163:1201–1210.
60 Ryan TA: NCAM and vesicle cycling: the importance of good glue in the long run. Neuron 2001;32:759–761.
61 Polo-Parada L, Bose CM, Landmesser LT: Alterations in transmission, vesicle dynamics, and transmitter release machinery at NCAM-deficient neuromuscular junctions. Neuron 2001;32:815–828.
62 Polo-Parada L, Bose CM, Plattner F, Landmesser LT: Distinct roles of different neural cell adhesion molecule (NCAM) isoforms in synaptic maturation revealed by analysis of NCAM 180 kDa isoform-deficient mice. J Neurosci 2004;24:1852–1864.
63 Dityatev A, Dityateva G, Schachner M: Synaptic strength as a function of post- versus presynaptic expression of the neural cell adhesion molecule NCAM. Neuron 2000;26: 207–217.
64 Stewart M, Popov V, Medvedev N, Gabbott P, Corbett N, Kraev I, Davies H: Dendritic spine and synapse morphological alterations induced by a neural cell adhesion molecule (NCAM) mimetic. Adv Exp Med Biol 2010; 663:373–383.
65 Muller D, Wang C, Skibo G, Toni N, Cremer H, Calaora V, Rougon G, Kiss JZ: PSA-NCAM is required for activity-induced synaptic plasticity. Neuron 1996;17:413–422.
66 Dityatev A, Dityateva G, Sytnyk V, Delling M, Toni N, Nikonenko I, Muller D, Schachner M: Polysialylated neural cell adhesion molecule promotes remodeling and formation of hippocampal synapses. J Neurosci 2004;24:9372–9382.
67 Bonfanti L: PSA-NCAM in mammalian structural plasticity and neurogenesis. Prog Neurobiol 2006;80:129–164.
68 Kochlamazashvili G, Senkov O, Grebenyuk S, Robinson C, Xiao M-F, Stummeyer K, Gerardy-Schahn R, Engel AK, Feig L, Semyanov A, Suppiramaniam V, Schachner M, Dityatev A: Neural cell adhesion molecule-associated polysialic acid regulates synaptic plasticity and learning by restraining the signaling through GluN2B-containing NMDA receptors. J Neurosci 2010;30:4171–4183.
69 Sato C, Kitajima K: Disialic, oligosialic and polysialic acids: distribution, functions and related disease. J Biochem 2013;154:115–136.
70 Podestá MF, Yam P, Codagnone MG, Uccelli NA, Colman D, Reinés A: Distinctive PSA-NCAM and NCAM hallmarks in glutamate-induced dendritic atrophy and synaptic disassembly. PLoS One 2014;9:e108921.
71 Gilabert-Juan J, Castillo-Gomez E, Pérez-Rando M, Moltó MD, Nacher J: Chronic stress induces changes in the structure of interneurons and in the expression of molecules related to neuronal structural plasticity and inhibitory neurotransmission in the amygdala of adult mice. Exp Neurol 2011;232:33–40.
72 Calandreau L, Márquez C, Bisaz R, Fantin M, Sandi C: Differential impact of polysialyltransferase ST8SiaII and ST8SiaIV knockout on social interaction and aggression. Genes Brain Behav 2010;9:958–967.
73 Eastwood SL, Harrison PJ: Synaptic pathology in the anterior cingulate cortex in schizophrenia and mood disorders. A review and a Western blot study of synaptophysin, GAP-43 and the complexins. Brain Res Bull 2001; 55:569–578.
74 Kim KC, Kim P, Go HS, Choi CS, Park JH, Kim HJ, Jeon SJ, Campomayor dela Pena I, Han S, Cheong JH, Ryu JH, Shin CY: Male-specific alteration in excitatory post-synaptic development and social interaction in pre-natal valproic acid exposure model of autism spectrum disorder. J Neurochem 2013;124:832–843.
75 Thierry AM, Gioanni Y, Dégénétais E, Glowinski J: Hippocampo-prefrontal cortex pathway: anatomical and electrophysiological characteristics. Hippocampus 2000;10:411–419.

Downloaded by:
UCSF Library & CKM
169.230.243.252 - 4/23/2015 9:51:46 PM